Journal of Inflammation Research

Dovepress
Taylor & Francis Group

Open Access Full Text Article

ORIGINAL RESEARCH

Susceptibility Factor TNF-α Synergizes with *Polygonum multiflorum* to Drive Idiosyncratic Liver Injury in Mice by Disrupting Gut Microbiota Composition and Hepatic Metabolite Homeostasis

Dilireba Aimaier, WanQuan Bai, Yun Zhang, Xiang Li, Chen Ma, Jian Gu, Le Zhang

College of Pharmacy and Food, Southwest Minzu University, Chengdu, Sichuan, 610225, People's Republic of China

Correspondence: Le Zhang, Email zhangle_only@163.com

Background: *Polygonum multiflorum* (PM), known as a traditional Chinese herb renowned for its tonic properties, has been used medicinally for millennia. However, it has drawn attention significantly due to the potential to induce idiosyncratic drug-induced liver injury (IDILI) in recent years. Previous studies identified the TNF-α, the pro-inflammatory cytokine, as a key factor contributing to susceptibility to PM induced-IDILI (PM-IDILI). However, the effects by which TNF-α mediates PM-IDILI remain poorly understood.

Methods: This study sought to elucidate the role of TNF-α in PM-IDILI using a TNF-α-sensitized C57BL/6J mouse model, integrating analyses of the gut microbiota and metabolomics We employed biochemical analysis, inflammatory markers, inflammatory liver histopathological, sequencing of 16S rRNA gene, as well as untargeted metabolomics based on LC-MS to systematically evaluate the extent of liver injury and characterize alterations in gut microbiota and liver metabolites following PM administration in TNF-α pre-treated mice.

Results: The results demonstrated that PM treatment in TNF-α-sensitized mice significantly elevated levels of indicators as AST (3.6-fold compared to the control group, $P < 0.05$) and ALT (3.9-fold compared to the control group, $P < 0.01$), increased plasma levels of IL-6 and IL-1β ($P < 0.05$ or $P < 0.01$), induced infiltration of inflammatory cell substantially in the liver. TNF-α-mediated PM disrupted the intestinal microbiota structure, characterized by reduced abundance of *Akkermansia* and increased abundance of *Lachnospiraceae_NK4A136_group, Bacteroides, Alloprevotella*, and *Blautia*. Furthermore, hepatic metabolomics analysis revealed that significant perturbations in TNF-α + PM treated mice, particularly affecting glutathione metabolism, purine metabolism, and arachidonic acid metabolism pathways.

Conclusion: These findings suggest that TNF-α sensitization predisposes mice to PM-IDILI, potentially by disrupting gut microbial homeostasis and altering host hepatic metabolism. This research provides critical theoretical and experimental evidence relevant to the safe and effective clinical application of PM.

Keywords: Polygonum multiflorum, TNF-α, idiosyncratic drug-induced liver injury, gut microbiota, metabolomics, susceptibility

Introduction

[1–3]Idiosyncratic drug-induced liver injury (IDILI) represents a substantial clinical challenge due to its unpredictable occurrence and heterogeneous manifestations. It manifests in a small subset of individuals who are exposed to certain medications, IDILI can lead to severe outcomes, including acute liver failure and potentially death.[4] The idiosyncrasy of IDILI poses significant hurdles for both clinical drug use and pharmaceutical development.[5] Although the precise pathogenesis of IDILI remains incompletely understood,[6–9] current evidence suggests it arises from complex interactions

Received: 5 April 2025
Accepted: 10 July 2025
Published: 17 July 2025

Graphical Abstract

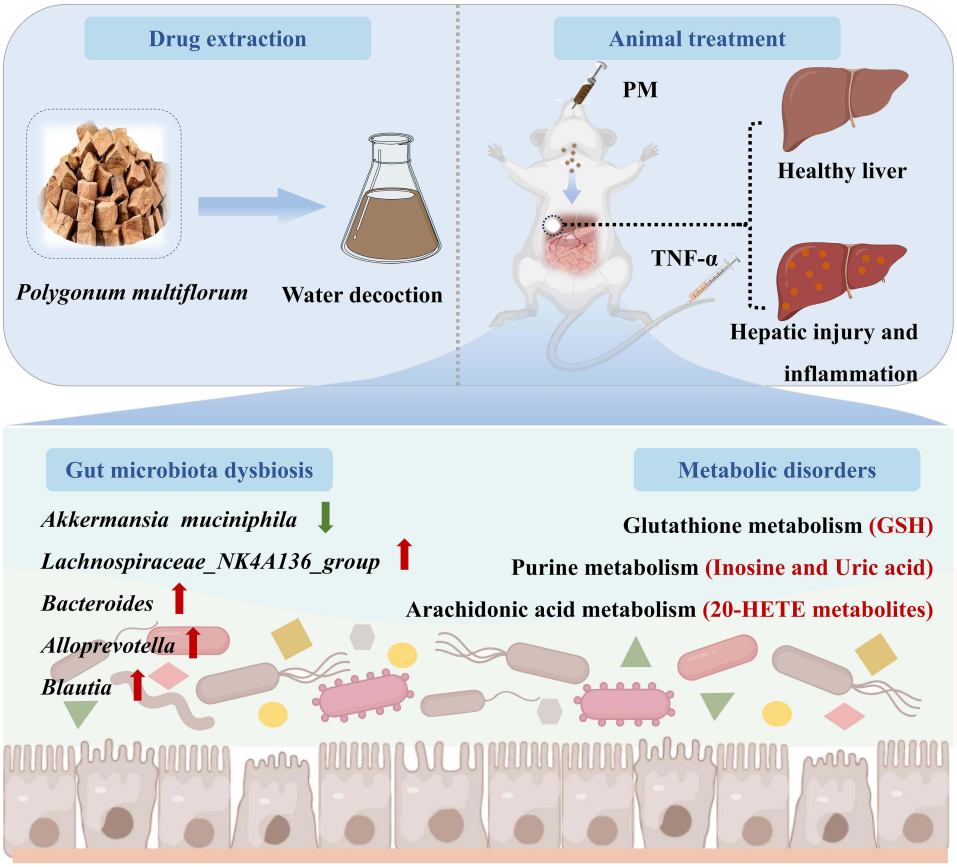

between drugs and host-specific factors, including genetic predispositions, underlying diseases, and the immune status, which collectively determine individual susceptibility and clinical phenotypes.

Polygonum multiflorum Thunb. (PM), derived from the dried tuberous roots of the Polygonaceae plant, is a well-known traditional Chinese medicine. It boasts a long history of use for centuries to nourish the liver and kidneys, enhance hematopoiesis, and promote musculoskeletal health.[10] Despite its widespread application in clinical settings and health supplements.[11,12] However, numerous reports linking PM consumption to liver injury have emerged globally in recent years, raising serious safety concerns.[13–17] Extensive research has demonstrated hepatotoxic potential in recent years, with injury patterns exhibiting immune-mediated idiosyncratic characteristics.[18,19] The immune-related factors, encompassing both congenital genetic variations and acquired individual immune stress, are implicated. Specifically, the activation of tumor necrosis factor-α (TNF-α), the pro-inflammatory cytokine, is closely related to the vulnerability to PM-induced liver injury. Critically, the role of TNF-α in PM-IDILI remains unclear.[20] While TNF-α activation is linked to susceptibility in PM-induced liver injury, the factors driving this vulnerability are unknown. We hypothesize that TNF-α exacerbates PM-induced liver injury via gut microbiota-metabolite dysregulation, bridging immune activation with microbial and metabolic disruptions.

The intestinal microbiome, the complex community of microorganisms inhabiting the digestive tract, influences host physiology and pathology profoundly by assessing alterations in the diversity and abundance of gut microbiome.[21–23] Analysis of the intestinal microbiome has become crucial for understanding the pathogenesis of various conditions, including the early strategy for diagnosis and treatment of drug-induced liver injury, inflammatory bowel disease, and metabolic syndrome. Metabolomics systematically analyzes the dynamic changes of small molecule metabolites in organisms to reveal the internal relationship between metabolic pathways and the occurrence and development of liver disease pathophysiology.

Prior studies have relied on single-omics approaches (eg, microbiome or metabolomics), limiting insights into systemic interactions.[24–26] Currently, the integrated approach of the gut microbiome and metabolomics has significantly contributed to elucidating host-microbial interactions, metabolic regulatory networks, and potentially discovering disease biomarkers.[27] Studies indicate that intestinal microbiome disruptions can influence host metabolic homeostasis, for example, through altered metabolism of bile acid or short-chain fatty acid production, thereby participating in the pathological progression of various liver diseases. Therefore, this study employed an integrative multi-omics strategy (16S rRNA sequencing + untargeted metabolomics) to decode the TNF-α/PM-gut-liver axis. This approach reveals how TNF-α synergizes with PM to alter microbial communities and host metabolites, offering mechanistic insights for safer PM clinical use.

Materials and Methods

Preparation of PM Water Decoction

Raw *Polygonum multiflorum* (PM) decoction pieces (Lot#20221204) were procured from Sichuan Yuanshangcao Traditional Chinese Medicine Decoction Co., Ltd (Sichuan, China). The quality of the material conformed to the standards outlined in the Chinese Pharmacopoeia (2020 edition). To prepare the extract, PM raw material (1 g) was decocted with 10 volumes (10 mL) of deionized water for 1 h. This extraction process was repeated twice more (total of three extractions). Subsequently, these decoctions were amalgamated, filtered through two layers of gauze, concentrated under negative pressure, and then lyophilized to generate a brown powder. Prior to administration, this lyophilized powder was reconstituted with deionized water to the required concentrations.

High Performance Liquid Chromatography (HPLC) Analysis of PM

HPLC analysis was conducted using an Agilent 1260 HPLC system equipped with a diode array detector. The separation of chemical constituents was achieved using an Agilent Eclipse Plus C18 analytical column (250 mm × 4.6 mm, 5 μm) maintained at 30 °C. The mobile phase consisted of methanol (Phase A) and water containing 0.1% formic acid (Phase B). The elution procedure was optimized as follows:

0–10 min, with 95–75% B.
10–20 min, with 75–50% B.
20–30 min, with 50–30% B.
30–35 min, with 30–20% B.
35–40 min, with 20–10% B.
40–45 min, with 10% B.

The flow rate of 1 mL/min was maintained, with the injection volume of 10 μL. UV detection was performed at 254 nm.

Animal Treatment

Forty-eight female C57BL/6J mice (18–20 g), specific pathogen-free, were obtained from SPF Biotechnology Co., Ltd (Beijing, China, License no. SCXK-(jing)2019–0010). The mice were acclimatized under controlled conditions, with a 12h light/dark cycle at a constant temperature of 25±2 °C. They were provided with ad libitum, standard chow and water. The animal study protocol was conducted in compliance with the National Research Council's Guide for the Care and all animal experimental procedures were reviewed and approved by the Animal Ethics Committee of Southwest Minzu University (Approval No. SMU-202401130).

After the one-week, acclimatization period, the mice were randomly allocated into six experimental groups (n=8 per group):

1. Normal Control (N): Vehicle treatment only.
2. Low-dose PM (PL): PM water decoction at 3.12 g/kg.
3. High-dose PM (PH): PM water decoction at 6.24 g/kg.
4. TNF-α Control (T): Recombinant murine TNF-α only.
5. TNF-α + Low-dose PM (TPL): TNF-α and low-dose PM co-administration.
6. TNF-α + High-dose PM (TPH): TNF-α and high-dose PM co-administration.

Recombinant murine TNF-α (Lot# 315–01A-100ug, sourced from *E. coli*, PeproTech Inc., NJ, US) was dissolved in sterile normal saline and administered at a dose of 10 ng/g body weight,[20] the dose of TNF-α administered was selected by a previous experimental study. The PM doses (3.12 g/kg and 6.24 g/kg, based on lyophilized powder weight) correspond to approximately 4 and 8 times the human clinical equivalent dose, respectively.

The treatment schedule (illustrated in Figure 1A) was as follows:

- Day 1: Mice in the T, TPL, and TPH groups were administered an intravenous (i.v). injection of TNF-α solution via the tail vein. For comparison, mice in the N, PL, and PH groups received an equivalent volume of saline vehicle i.v. Two hours later, mice in the PL, PH, TPL, and TPH groups received the corresponding dose of PM water decoction via oral gavage (intragastric administration). Mice in the N and T groups received an equivalent volume of deionized water vehicle via oral gavage.
- Days 2–6: Mice received their respective daily treatments (PM decoction or water vehicle) via oral gavage.
- Day 7: The treatment regimen from Day 1 (i.v. injection followed 2 hours later by oral gavage) was repeated.

Sample Collection

Seven hours after the final administration, fecal samples were collected from each mouse under sterile conditions (within a clean bench), and immersed rapidly in liquid nitrogen until further analysis. Subsequently, all of the mice were anaesthetized using 1.5% isoflurane inhalation. The it collected the blood via the retro-orbital plexus into appropriate tubes. Plasma was separated by centrifugation after allowing the blood to clot and preserved at −80 °C until further analysis. Part of the left lateral lobe was fixed in 4% paraformaldehyde solution for the histological examination. The remaining liver tissue was in liquid nitrogen snap-frozen and stored at −80 °C for further analysis.

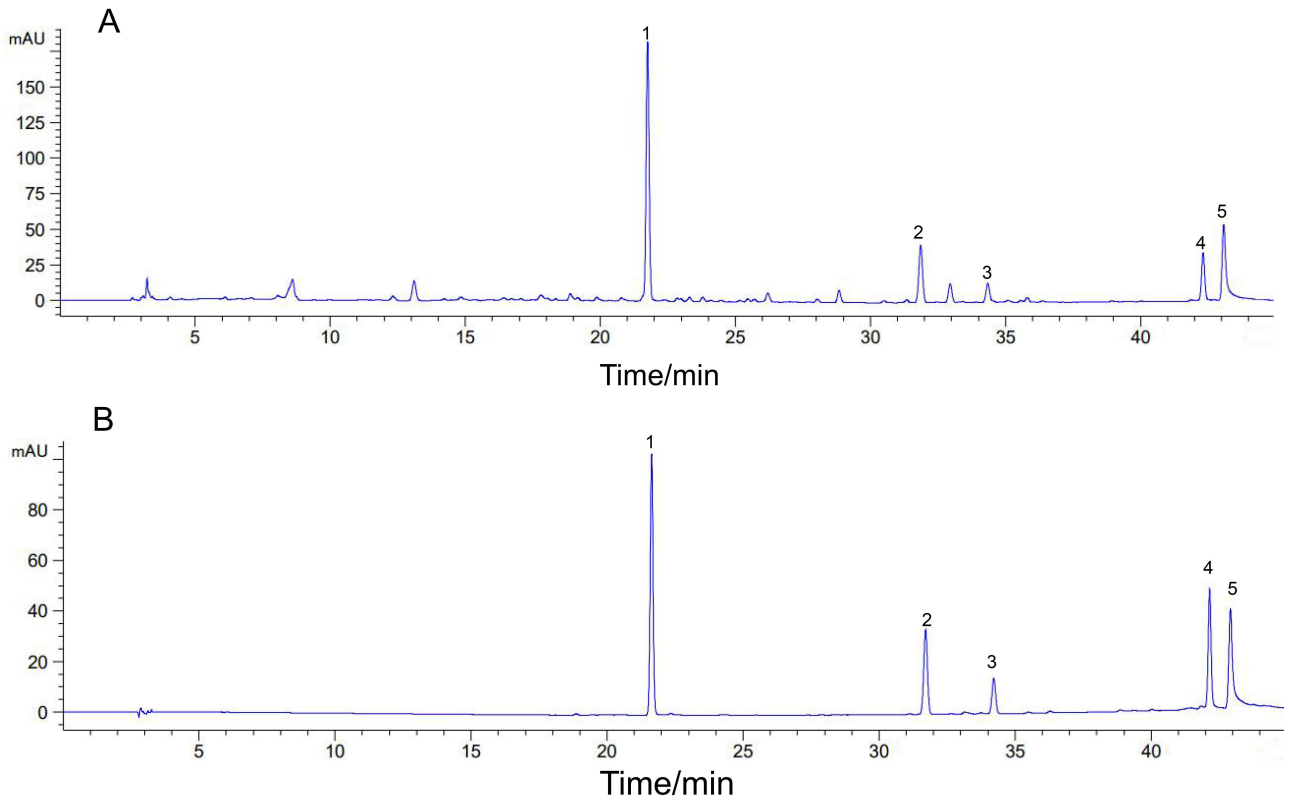

Figure 1 Chromatograms of PM decoction (**A**) and five mixed reference standards (**B**). 1: TSG; 2: E8OG; 3: P8OG; 4: emodin; 5: physcion.

Plasma Biochemical and Histological Analysis

Plasma levels of ALT and AST were detected through commercial diagnostic kits (AST by Cat# C010-2-1; ALT by Cat# C009-2-1; Nanjing Jiancheng Bioengineering Institute, Nanjing, China) according to the instructions for manufacturer.

The anterior portion of the left lateral lobe of the liver was sectioned fixed in 4% paraformaldehyde for 48 hours. After fixation, the sample was then embedded in paraffin, sectioned into 5 μm sections, and stained with hematoxylin and eosin (H&E) to evaluate liver pathology under the microscope.

Determination of Plasma IL-6 and IL-1β

The plasma levels of IL-6 and IL-1β were assessed using the Mouse IL-6 High Sensitivity ELISA Kit (Cat# EK206HS; Multisciences) and the Mouse IL-1β High Sensitivity ELISA Kit (Cat# EK201BHS; Multisciences) following the manufacturer's instructions. Results are reported in pg/mL.

16S rRNA Gene Sequencing for Analysis of Microbiota

Total microbial DNA was extracted from the collected fecal samples using The NEBNext Ultra II DNA Library Prep Kit (Cat# E7645B; New England Biolabs) following the manufacturer's protocol. The specific steps were DNA extraction, design of primers and junctions, polymerase chain reaction (PCR) amplification (Thermal cycling consisted of initial denaturation at 98°C for 1 min, followed by 30 cycles of denaturation at 98 °C for 10s, annealing at 50 °C for 30s, and elongation at 72 °C for 30s and 72 °C for 5 min), quantification and equal mass mixing, end repair, A-addition, junction ligation, library construction and sequencing. According to standard protocols, the 16S rRNA gene sequencing data were analyzed on the Illumina NovaSeq platform The constructed libraries were subjected to Qubit and Q-PCR quantitative quality control. Up-sequencing was performed on the NovaSeq 6000. Alpha diversity metrics (eg, observed operational taxonomic units, Shannon, Simpson and Chao1 indices) were calculated to assess within sample diversity. Beta diversity, reflecting between-sample community structure variation, was visualized using principal coordinate analysis (PCoA).

Metabolomics Analysis

Sample Preparation and UPLC–MS/MS Analysis

A 100 mg liver tissue sample was ground by liquid nitrogen. Metabolites were extracted by adding 500 μL of 80% methanol in water, followed by vortexing for 3 min. The mixture was then sonicated, vortexed again, and allowed to stand for 5 min in an ice bath before centrifugation at 15000 r/min, 4 °C, for 20 min. An aliquot of supernatant was diluted with mass spectrometry grade water to achieve the methanol concentration of 53%. This diluted mixture was re-centrifuged (15,000 rpm, 20 min, 4 °C) to remove any potential precipitates. The final supernatant from each sample was collected and injected into LC-MS for analysis. To monitor the stability and repeatability of instrument, liver tissue sample was taken and mixed as the quality control (QC) sample. The QC sample was inserted regularly and analyzed in every eight samples to ensure instrument stability during the analytical process.

The chromatographic separation was performed on a Hypersil Gold column (C18) (100×2.1 mm, 1.9 μm). Mass spectrometric analysis was conducted using a Q Exactive™ HF/Q Exactive™ HF-X mass spectrometer equipped with an electrospray ionization (ESI) source operating in both positive and negative ion modes. The specific conditions for chromatographic and mass spectrometric analyses are detailed in the supplementary information 1.

Data Processing and Multivariate Statistical Analysis

The data processing and analysis were performed using the CD 3.3 compound discovery software. The raw data underwent peak detection, peak alignment, and retention time correction to obtain mass-to-charge ratios (m/z), retention times, and peak areas. After normalization procedures, metabolites with coefficient of variation (CV) <30% in QC samples were selected, yielding identified metabolites and their relative quantification results.

The processed data were then imported into the metaX metabolomics analysis platform for multivariate statistical analysis, including principal component analysis (PCA) and partial least squares-discriminant analysis (PLS-DA), which generated variable importance in projection (VIP) scores for each metabolite. For univariate analysis, two-sample *t*-tests

were performed to assess the statistical significance (P-value) of each metabolite between groups, along with fold change (FC) calculations.

The screening criteria for differential metabolites were set as: VIP >1, P-value <0.05, and absolute FC ≥2 or FC ≤0.5. This comprehensive analytical workflow ensured rigorous identification of significantly altered metabolites between experimental groups.

Statistical Analysis

Data were statistically analyzed through the software GraphPad Prism 8.0. The results obtained were expressed in the form of mean ± SD or mean ± SEM. Comparisons between two groups were analyzed using an unpaired Student's *t*-test. Comparisons among three or more groups were performed using one-way analysis of variance (ANOVA). P-value < 0.05 was considered statistically significant.

Results

Quantitative Analysis of Representative Compounds in PM Detection

HPLC was employed to quantify five characteristic compounds within the prepared *Polygonum multiflorum* (PM) (Figure 2). The following compounds were identified and quantified through the comparison of retention times and ultraviolet spectra against authentic reference standards: 2,3,5,4′-tetrahydroxystilbene-2-O-β-D-glucoside (TSG), physcion-8-O-β-D-glucoside (P8OG), emodin-8-O-β-D-glucoside (E8OG), emodin, and physcion. According to the results of the HPLC determination, the contents of the above five components in the water decoction of PM were 35 mg/g of TSG, 2.9 mg/g of E80G, 0.7 mg/g of P8OG, 0.9 mg/g of emodin, and 0.7 mg/g of physcion, respectively. The chromatograms of the individual compounds are detailed in Figure S1.

Co-Administration of TNF-α and PM Water Decoction Exacerbated Pathological Damage and Inflammation of Liver Tissue

To evaluate the plasma ALT and AST level in mice in the TPL and TPH groups measured. Compared to the N group, mice receiving both TNF-α and PM (TPL and TPH groups) displayed significantly elevated plasma AST and ALT levels (Figure 3B and C, Table S1; $P < 0.05$ or $P < 0.01$). Treatment with TNF-α alone (T group) caused only a minor, non-significant increase in these liver enzymes, whereas administration of PM decoction alone (PL and PH groups) resulted in ALT and AST levels comparable to the control group. These biochemical results strongly suggest that TNF-α increases the sensitivity of PM-DILI, acting as a critical susceptibility factor.

As shown in Figure 3D, compared with the N group, all other experimental groups exhibited elevated IL-6 levels, with statistically significant increases observed in the TPL, Tand TPH groups ($P < 0.05$ or $P < 0.01$). Notably, the TPH group demonstrated a more pronounced upward trend relative to both the T and TPL groups. Similarly, Figure 3E revealed that compared to the N group, the PL, PH, T, TPL, and TPH groups all showed increased IL-1β levels, with the TPH group displaying statistically significant elevation versus all other groups ($P < 0.01$).

As shown in Figure 3F, the sections of liver from the N, PL, and PH groups, generally exhibited normal hepatic architecture, showing intact lobular structures with hepatocytes arranged radially around the central vein as the center. There was occasional infiltration of inflammatory cells, while no obvious pathological changes were observed. Compared to the N group, the T group, in which the cytokine TNF-α was administered alone, exhibited minimal inflammatory cell infiltration in the confluent region of the liver tissue, but lacked histopathological changes. In stark contrast, in the liver tissues from the TPL and TPH groups showed marked pathological alternations, including central venous dilation, intimal shedding, and significant infiltration of inflammatory cells, particularly concentrated within the portal tracts (It has been indicated by arrows in the Figure 3F).

Impact of Co-Administration of PM and TNF-α on Gut Microbial Composition

We next investigated gut microbial community alterations using 16S rRNA gene sequencing of cecal contents, as shown in Figure 1A and C. The species rank-abundance distribution curves suggested sufficient sequencing depth across all

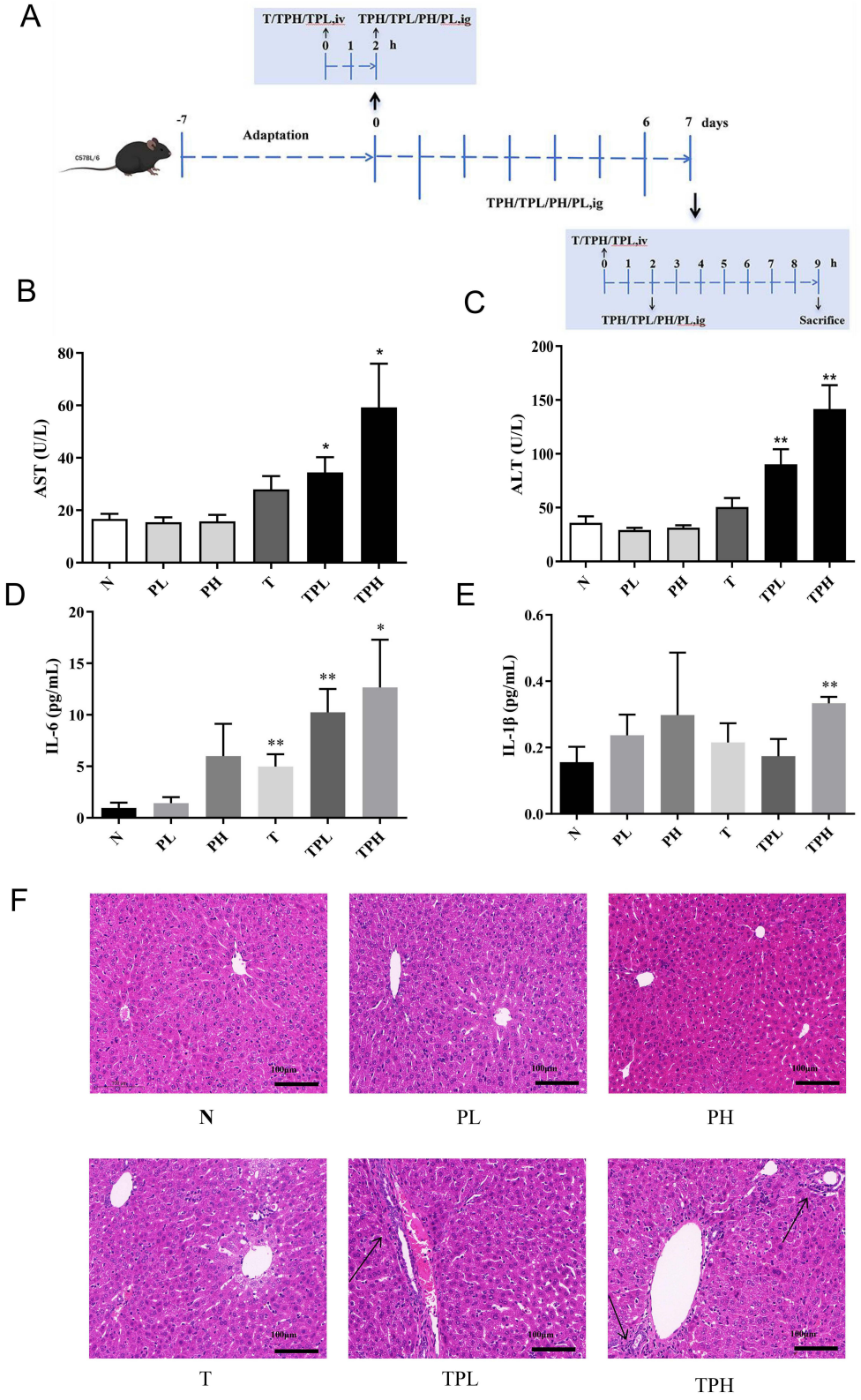

Figure 2 Effects of co-administration of TNF-α and PM on mouse liver. (**A**) Experimental design of animal studies. (**B**) Plasma level of AST. (**C**) Plasma level of ALT. (**D**) Plasma level of IL-6. (**E**) Plasma level of IL-1β. Data are means ± SEM. Significant differences indicated as: *$P < 0.05$, **$P < 0.01$ vs N group. (**F**) Pathological changes in liver tissue. Scale bar = 100 μm. (A-F, n = 8).

https://doi.org/10.2147/JIR.S528667

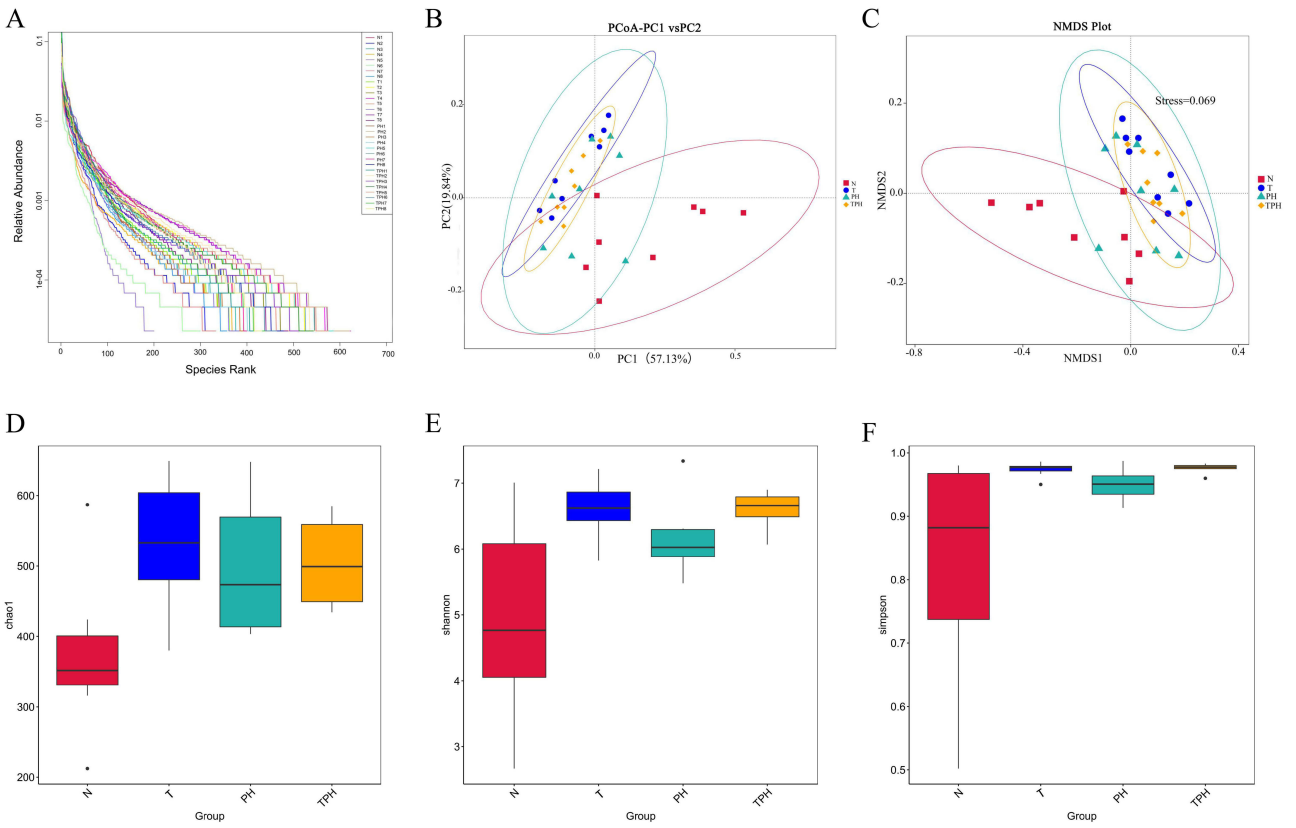

Figure 3 Co-administration of TNF-α and PM water decoction modulates the diversity of the gut microbiome in mice. (**A**) The Rank Abundance plot in each group. (**B**) PcoA analysis on intestinal microbiota. (**C**) NMDS analysis on intestinal microbiota. Alpha diversity indicates microbiota in the faecal contents of mice. (**D**) Chao1 index; (**E**) Shannon index; (**F**) Simpson index; Data are means ± SD. (A-F, n = 8).

samples (Figure 1A). PCoA and NMDS based on Bray-Curtis distance showed that the co-administration of TNF-α and PM altered the structure of the intestinal flora significantly. The Simpson index showed no significant difference between the N and TPH groups (Figure 1F). However, both the Shannon and Chao1 index indices were significantly elevated in the TPH group relative to the N group (Figure 3D and E). It suggests that the combined TNF-α and PM treatment contributed to higher microbiota diversity.

As shown in Figure 4a–f, each group had a different combination of microorganisms at the phylum, class, order, family, genus, and species level (the top 10 classifications with the highest abundance were selected). At the level of gut microbial families in each group (Figure 4d), *Verrucomicrobiota* abundance was higher in the N group of mice relative to the T, PH and TPH group, *Bacteroidota* was significantly enriched in all four groups: N, T, PH, and TPH, but the enrichment degree was the highest in the TPH group. At the genus level, *Akkermansia* abundance was significantly higher in the N group of mice, whereas *Lachnospiraceae_NK4A136_group, Bacteroides, Alloprevotella*, and *Blautia* abundances were relatively lower. T, PH, and TPH groups all showed a relative increase in *Lachnospiraceae_NK4A136_group, Bacteroides, Alloprevotella*, and *Blautia* and a relative decrease in *Akkermansia*, the most significant change was observed in the TPH group (Figure 4e).

In order to identify specific bacterial communities in the different groups, we performed LEfSe analysis on all samples (LDA >4) and obtained histograms of the distribution of LDA values and evolutionary maps (Figure 5A and B). The LDA scores showed differences in 6, 4, 9, and 2 bacterial species in the N, PH, T, and TPH groups, respectively.

In conclusion, co-administration of TNF-α with PM profoundly alters the gut microbial composition in mice. The increase of *Akkermansia* abundance and the decrease of *Lachnospiraceae_NK4A136_group* abundance, may contribute to the mechanism underlying TNF-α-mediated susceptibility to PM- IDILI.

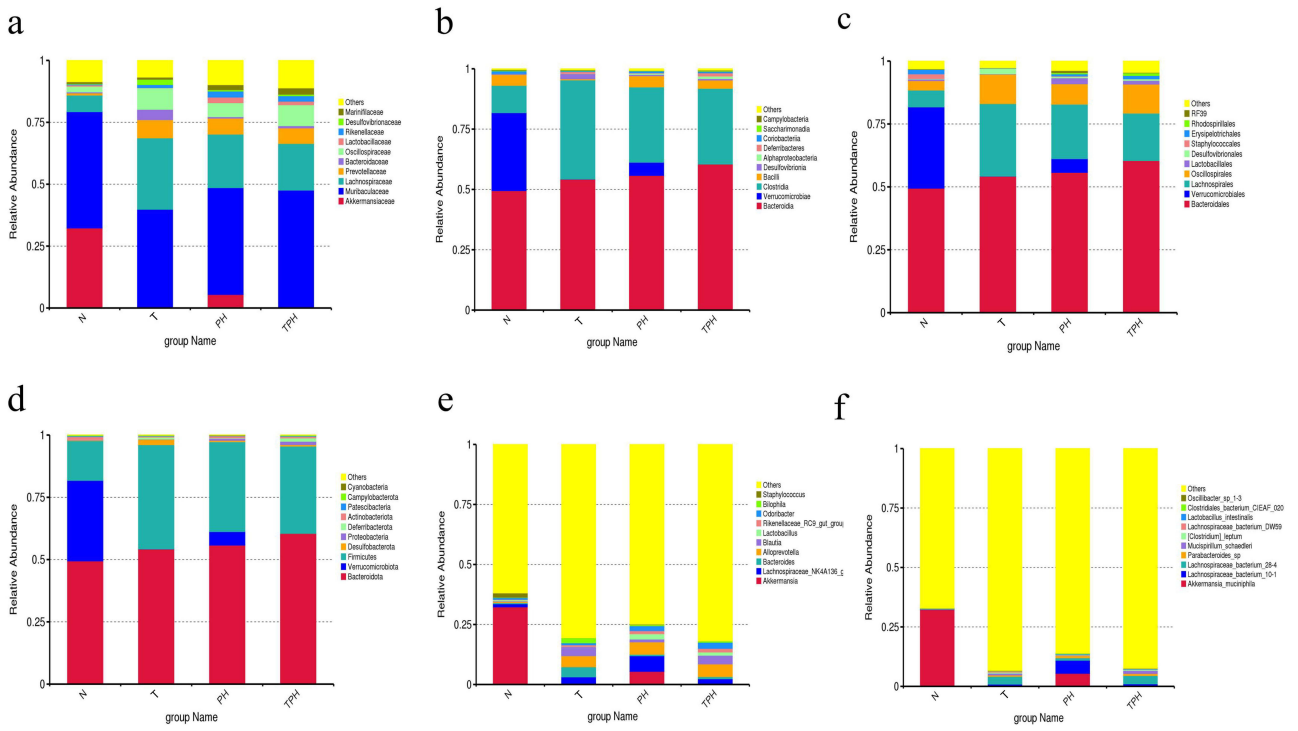

Figure 4 Proportion of intestinal microbes in N, T, PH and TPH groups. (**a**) Phylum level relative abundance. (**b**) Class level relative abundance. (**c**) Order level relative abundance. (**d**) Family level relative abundance. (**e**) Genus level relative abundance. (**f**) Species level relative abundance. Data are means ± SD. (x±s, n=8).

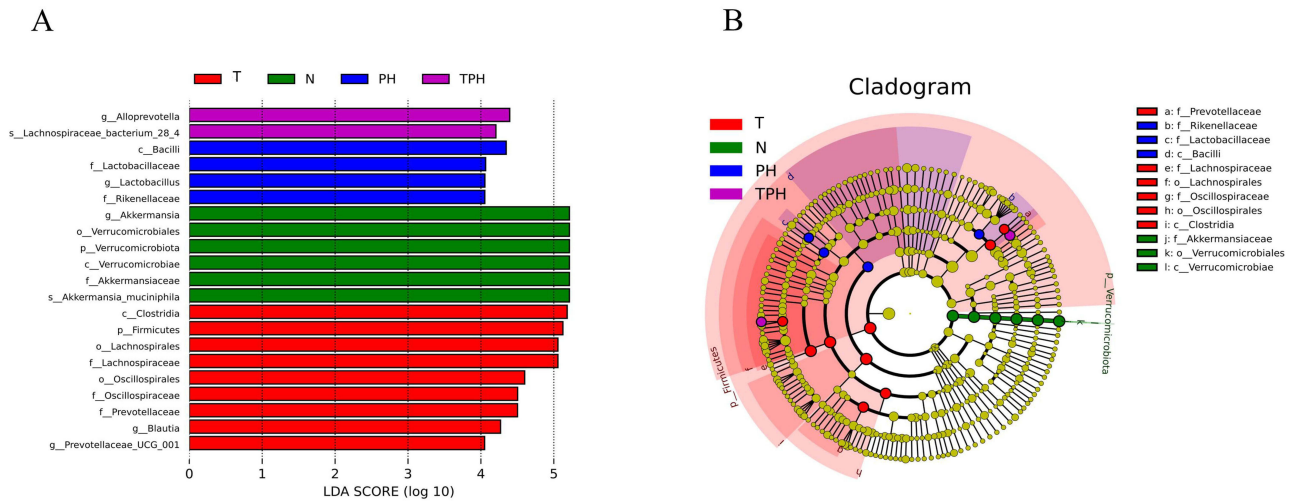

Figure 5 Linear discriminant analysis effect size (LEfSe) analysis was conducted on intestinal flora of mice in each group. (**A**) LEfSe analysis highlighted the dominant biomarker taxa in the four groups (LDA score > 4). (**B**) Taxonomic cladogram derived from LEfSe analysis (LDA score>4, n=8 per group).

Effects of Co-Administration of PM and TNF-α on Liver Metabolome

Initial unsupervised Principal Component Analysis (PCA) of liver lobule tissue samples from each group of mice in both positive and negative ion modes, thereby confirming the stability and reliability of the analytical platform (Figure 6A and B). The dots representing the QC group were mostly concentrated around the origin of the axes, suggesting that the LC-MS system was stable and reliable in the overall analysis process. Importantly, PCA revealed a clear distinction of metabolic profiles between the N, T, PH, and TPH groups, indicating significant treatment-induced alterations in the fecal metabolome.

https://doi.org/10.2147/JIR.S528667

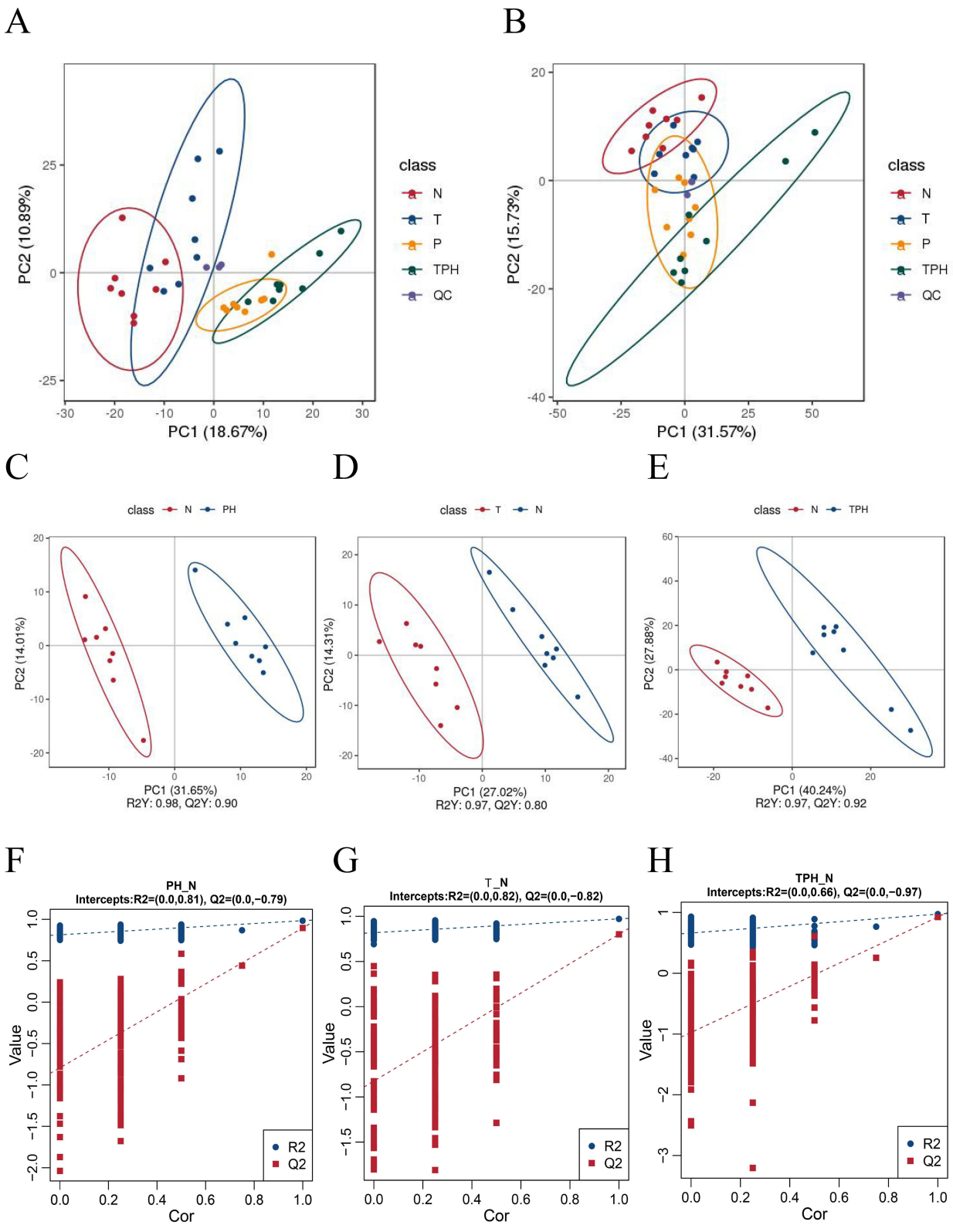

Figure 6 Metabolic profile and multivariate analysis among the four groups. (**A**) PCA score plot (positive ion mode). (**B**) PCA score plot (negative ion mode). (**C**) OPLS-DA score plot (N vs PH) (**D**) OPLS-DA score plot (N vs T). (**E**) OPLS-DA score plot (N vs TPH). (**F**) Permutation tested for OPLS-DA model (N vs PH). (**G**) Permutation test for OPLS-DA model (N vs T). (**H**) Permutation tested for OPLS-DA model (N vs TPH).

In addition, OPLS-DA model was applied for the analysis to further distinguish the differences in the metabolic environment. The sub-matrix projections of the samples from each group are shown below, and the groups are clearly separated, demonstrating significant differences in endogenous metabolites among the groups. The explanatory parameter ability of the model, R2Y, was 0.98, 0.97, 0.97, respectively according to the constructed OPLS-DA model; the predictive ability parameter, Q2, was 0.90, 0.80, 0.92, respectively; and the R2Y/Q2 was 1.08, 1.21, 1.05, respectively, which were close to 1, proving that the model differentiation and prediction instincts were relatively good, as shown below in Figure 6C–E. The OPLS-DA models demonstrated good statistical performance, with high R2Y values and Q2 values. Model validity was further confirmed through permutation tests (200 permutations). All Q2 (R2) were lower than the original values on the right, and the dark blue regression line where Q2 was located intersected the left vertical coordinate below zero, which showed that the observed separations were statistically significant (Figure 6F–H).

To facilitate further screening and identification of differential metabolites, we initially employed OPLS-DA models. This was followed by univariate analysis to investigate the variable differences between the PM water decoction alone group (PH group), the TNF-α alone group (T group), and the combined treatment group (TPH group) comparing to the normal control group (N group), under both positive and negative ion modes respectively. The criteria for selection were set as: VIP >1, $P < 0.05$, and FC >2 or FC<0.5. Variables meeting these thresholds were designated as significantly altered differential metabolites between the groups. The overlap among these screened differential metabolites was subsequently analyzed using a Venn diagram (refer to Figure 7A).

The results indicated that the administration of PM water decoction alone induced significant changes in 258 metabolites in mice (PH vs N). Similarly, the dosing of the immune cytokine TNF-α alone led to significant alterations in 149 metabolites (T vs N). However, the combined dosing of TNF-α and PM water decoction result in significant modifications in 326 metabolites (TPH vs N). Notably, 125 differential metabolites in the TPH group vs the N group were indicated that did not overlap with those found in either the PH vs N or T vs N comparisons. This finding suggests that these differential metabolites were affected by the synergistic damaging effects of TNF-α and PM water decoction, instead of the individual pharmacological effects of PM water decoction or TNF-α alone. Therefore, these 125 differential variables can be considered as potential metabolites that signify the specific metabolic pathways involved in liver injury prompted by the synergistic interaction between the PM water decoction and the susceptibility factor TNF-α in mice.

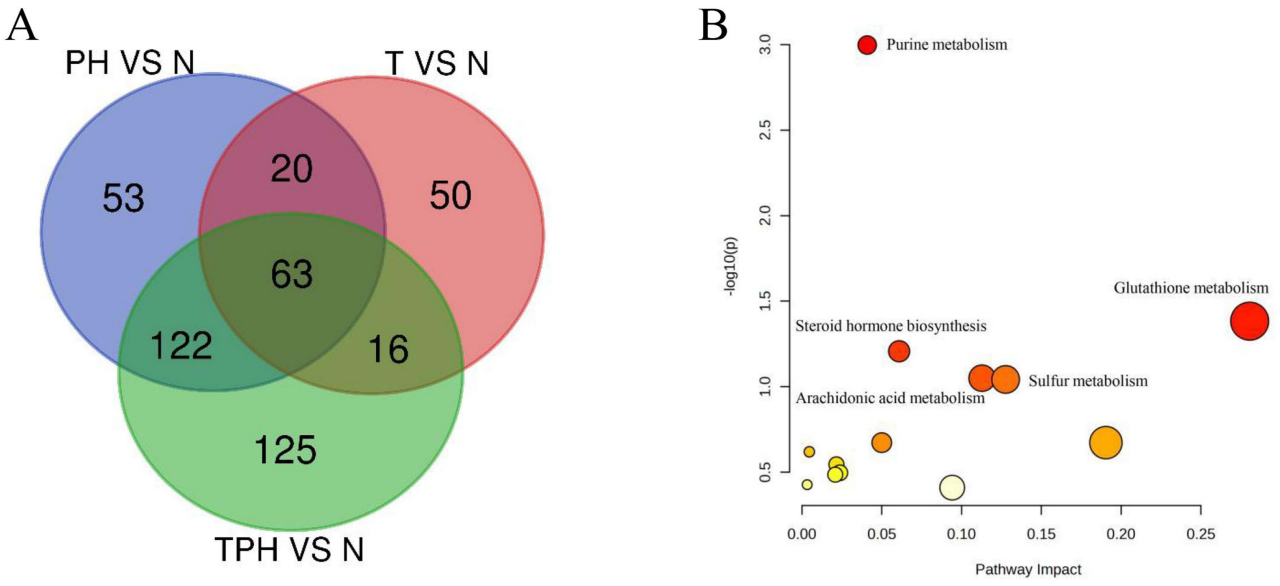

Figure 7 Screening for differential metabolites and pathways enrichment analysis associated with liver injury. (**A**) Venn diagram showing differential metabolites in comparisons of the N group with the PH, T, and TPH groups. (**B**) Analysis of metabolic pathways of biomarkers.

https://doi.org/10.2147/JIR.S528667

Subsequently, the identities of these potential metabolites associated with PM-DILI were confirmed using the Metlin database. Leveraging the acquired KEGG IDs, metabolic pathway analysis was then carried out employing the online analysis software MetaboAnalyst. After removing drug exogenous metabolites as well as duplicate values, a total of 18 potential endogenous metabolites were matched, including cis-Aconitic acid, Deoxycytidine, D-Erythrose4-phosphate, Adenosine diphosphate, Uric acid, gamma-Glutamylcysteine, 3′-DephosphocoenzymeA, Aldosterone, Hydrocortisone acetate, ProstaglandinH2, 20-hydroxy-eicosatetraenoic acid, Adenylylsulfate, L-Glutathione (reduced), Inosine, Adenylosuccinic acid, L-Kynurenine, Methylthioadenosine, Dehydroepiandrosterone, and the metabolite details are shown in Table 1.

Based on the analysis of 18 differential metabolites identified above by metaboanalyst 6.0 official website for metabolic pathway analysis, and the metabolic pathways of PM that synergistically interacted with susceptibility factors to cause liver injury in mice were enriched (Figure 7B and Table S2) The most prominently affected pathways included Purine metabolism, Glutathione metabolism, Steroid hormone biosynthesis, Arachidonic acid metabolism, Sulfur metabolism, and Citrate cycle, suggesting widespread metabolic disruption resulting from the combined action of TNF-α and PM, Pantothenicacid metabolism, Pentose phosphate pathway include the metabolisms such as aspartate and glutamate, Glyoxylate and dicarboxylate, Cysteine and methionine, Pyrimidine, and Tryptophan metabolism.

Correlation Analysis of Liver Injury Markers, Liver Metabolites and Gut Microbiota

To investigate the potential functional links of the observed changes in liver injury markers, liver metabolites and gut microbiota, Spearman correlation analysis was conducted. As shown in Figure 8A, the heatmap suggests that *Akkermansia* and *Bacteroidota* are inversely associated with ALT/AST levels, consistent with their roles in maintaining gut-liver homeostasis. Conversely, *Prevotellaceae*, *Firmicutes* and *Lachnospiraceae_NK4A136_group* show positive correlations, aligning with their pro-inflammatory potential. Notably, as shown in Figure 8B, *Akkermansia* was significantly positively correlated with Uric acid, 3′-Dephosphocoenzyme A, reduced L-Glutathione, and gamma-Glutamylcysteine, while being negatively correlated with Adenylyl Sulfate and Aldosterone.

Table 1 Differential Metabolites of PM Causing Idiosyncratic Liver Injury

NO	RT (min)	KEGG ID	Metabolites	Formula	M/Z	TPH vs N		
						FC	*P* value	VIP
ESI−								
1	1.39	C00417	cis-Aconitic acid	$C_6H_6O_6$	173.0092	3.73	0.0258	1.1260
2	1.44	C21554	Deoxycytidine	$C_9H_{13}N_3O_4$	226.0837	2.86	0.0302	1.0858
3	1.45	C00279	D-Erythrose 4-phosphate	$C_4H_9O_7P$	199.0014	3.48	0.0142	1.0144
4	1.63	C00008	ADP	$C_{10}H_{15}N_5O_{10}P_2$	426.0227	2.46	0.0274	1.2299
5	1.89	C00366	Uric acid	$C_5H_4N_4O_3$	167.0210	11.64	0.0010	1.3102
6	1.97	C00669	Gamma-Glutamylcysteine	$C_8H_{14}N_2O_5S$	249.0552	4.94	0.0026	1.2212
7	5.59	C00882	3′-Dephosphocoenzyme A	$C_{21}H_{35}N_7O_{13}P_2S$	686.1435	14.07	0.0013	1.3024
8	6.31	C01780	Aldosterone	$C_{21}H_{28}O_5$	405.1922	0.09	0.0003	1.5526
9	6.65	C02821	Hydrocortisone acetate	$C_{23}H_{32}O_6$	403.2109	0.41	0.0030	1.1134
10	8.49	C00427	ProstaglandinH2	$C_{20}H_{32}O_5$	333.2075	0.27	0.0004	1.5016
11	9.16	C14748	20-HETE	$C_{20}H_{32}O_3$	319.2280	0.31	0.0025	1.3751
ESI^+								
12	1.40	C00224	Adenylylsulfate	$C_{10}H_{14}N_5O_{10}PS$	428.0291	0.18	0.0000	1.7110
13	1.85	C00051	L-Glutathione(reduced)	$C_{10}H_{17}N_3O_6S$	308.0909	3.11	0.0000	1.4031
14	3.26	C00294	Inosine	$C_{10}H_{12}N_4O_5$	269.0881	2.61	0.0000	1.4156
15	4.72	C03794	Adenylosuccinic acid	$C_{14}H_{18}N_5O_{11}P$	464.0819	5.33	0.0001	1.6222
16	4.74	C00328	L-Kynurenine	$C_{10}H_{12}N_2O_3$	209.0924	0.36	0.0003	1.5949
17	5.17	C00170	Methylthioadenosine	$C_{11}H_{15}N_5O_3S$	298.0972	2.06	0.0005	1.5075
18	6.99	C01227	Dehydroepiandrosterone	$C_{19}H_{28}O_2$	271.2054	0.45	0.0354	1.2599

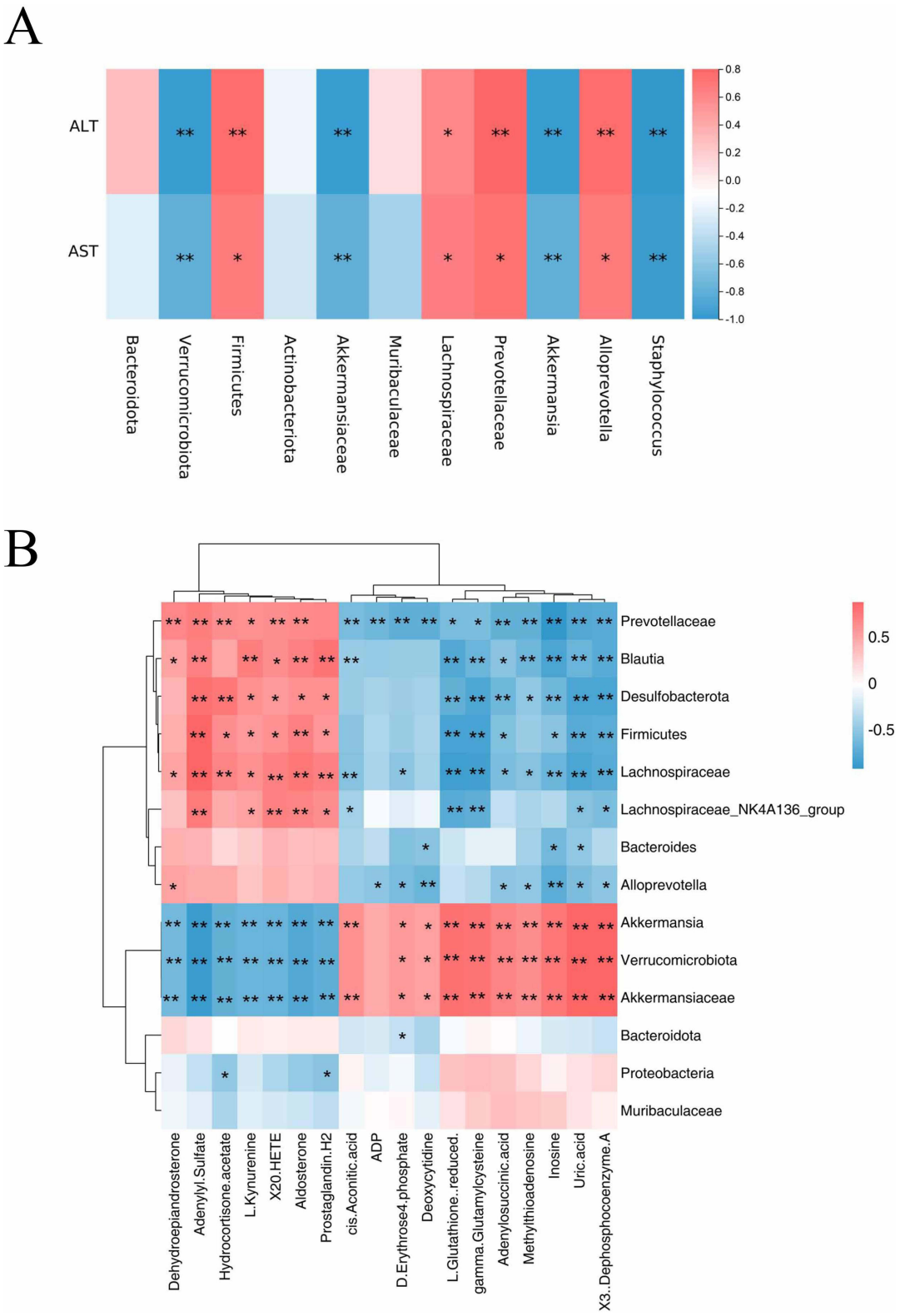

Figure 8 Spearman correlation heatmap of liver function markers, metabolomic profiles, and fecal microbiome dysbiosis. (**A**) The relationship between gut microbiota and liver enzymes (ALT/AST). (**B**) Correlation network of hepatic metabolic signatures, and differential gut Microbiota. Color intensity indicates the correlation coefficient (Red: positive, Blue: negative). (*$P < 0.05$; **$P < 0.01$).

https://doi.org/10.2147/JIR.S528667

Lachnospiraceae_NK4A136_group was positively correlated with Adenylyl Sulfate, and Aldosterone, while negatively correlated with L-Glutathione (reduced), gamma-Glutamylcysteine, Uric acid, and 3′-Dephosphocoenzyme A, among other metabolites.

Discussion

Although IDILI affects only a susceptible minority of individuals, it remains a significant cause of serious adverse reactions in clinical practice.[8] Predicting IDILI based on dose or known pharmacology is notoriously challenging due to its complex dependence on individual susceptibility factors.[18–20] Previous studies have established that PM-induced liver injury displays distinct idiosyncratic properties, with the immune disorder, specifically TNF-α activation, being a key determinant of susceptibility. Furthermore, studies have confirmed that TNF-α plays a critical role in (IDILI) caused by co-administration of ranitidine,[28] trovafloxacin,[29] sulindac,[30] amiodarone,[7] and LPS. However, it remains unclear how the host susceptibility factors interact with drugs to induce IDILI. Addressing this gap, studies utilized the TNF-α-induced mouse model of atypical liver injury to explore the mechanism of PM-induced liver injury from an endogenous point of view in combination with intestinal flora and metabolomics. Our findings demonstrated that mice in the TPH group treated with TNF-α and PM exhibited significantly elevated plasma AST and ALT levels (3.6- and 3.9-fold increases, $P<0.05$, $P<0.01$, respectively) compared with group N. Compared with the N group, inflammatory markers including IL-6 and IL-1β were significantly elevated in the TNF-α and PM co-exposure groups, with the most pronounced increase observed in the TNF-α plus high-dose PM combination group ($P < 0.05$, $P < 0.01$). Liver tissue sections from the TPH group showed a marked infiltration of inflammatory cells in the portal area. Conversely, administration of either TNF-α or PM alone did not induce significant biochemical or histological signs of liver injury compared to controls. This confirms that TNF-α sensitization markedly increases susceptibility to PM-induced liver damage, acting synergistically with the herb to trigger injury resembling IDILI.

[21] The gut-liver axis encompasses the crucial bidirectional interaction between the gastrointestinal tract, its microbiota, and liver.[31] Issues with gut barrier function can lead to the translocation of microorganisms into the bloodstream, inducing a sustained inflammatory response that promotes liver injury, liver fibrosis, cirrhosis, and liver cancer. Alterations in the gut microbial populations or their function are increasingly implicated in affecting health.[23] Recent research has increasingly linked alcohol-related liver disease, non-alcoholic fatty liver disease and autoimmune liver disease to modifications in the function and structure of the gut microbiota.[32–34] The interaction between gut microbiota and their metabolome with immune responses constitutes a highly dynamic and bidirectionally regulated process, involving a multi-layered immune-microbial network at the molecular level. Dysregulation of the microbiota structure (such as an increase in Gram-negative bacteria) can promote lipopolysaccharide (LPS) release, which activates the TLR4/NF-κB signaling pathway to induce macrophage overproduction of TNF-α. Conversely, commensal bacteria-derived short-chain fatty acids (such as butyric acid) suppress histone deacetylases (HDACs) and activate GPR43 receptors, thereby down-regulating the expression of TNF-α. Excessive TNF-α further disrupts intestinal epithelial tight junctions, leading to microbial translocation and metabolic disturbances (such as a reduction in secondary bile acids), thus forming a vicious cycle. These interactions are particularly prominent in autoimmune diseases and metabolic syndrome, with mechanistic insights offering novel therapeutic strategies targeting the microbiota-immune axis.

In this study, 16SrRNA gene sequencing analysis revealed distinct alterations in gut microbial community structure following drug administration. Beta diversity analysis clearly separated the TPH group from controls. Interestingly, alpha diversity metrics such as the Shannon and Simpson indices were significantly elevated in the TPH group, indicating that TNF-α-induced PM contributed to an increase in the α diversity of gut microbiota Five different species of bacteria were identified at the genus level: *Akkermansia, Lachnospiraceae_NK4A136_group, Bacteroides, Alloprevotella* and *Blautia*. These specific alterations suggest that the above bacteria play a crucial role in PM-induced IDILI under immune stress. Our research found that TNF-α preactivation significantly enhanced the perturbation effect of PM on the intestinal flora, which was mainly manifested as: the abundance of Akkermansia decreased and the abundance of Lachnospiraceae_NK4A136_group increased significantly.[35] Among them, *Akkermansia*, a Gram-negative bacterium residing in the phylum *Verrucomicrobium*, is generally considered beneficial. The lack or reduced abundance of this commensal bacterium has been linked to various metabolic and inflammatory disorders, including obesity, diabetes,

hepatic steatosis, and inflammation.[36] The abundance of *Akkermansia* showed negative correlation with liver injury, lipid metabolism, oxidative damage, and fibrosis in general.[35,37,38] It is also associated with the development of many liver diseases closely. Conversely, certain members of the *Lachnospiraceae* family, including the *Lachnospiraceae_NK4A136_group*, are sometimes considered opportunistic pathogens associated with inflammation, is found in high levels in diseases in conditions like nonalcoholic steatohepatitis and obesity. Our findings align with these general associations.

Currently, untargeted metabolomics provided further metabolites insights and is potentially able to elucidate the mechanisms by which TNF-α synergizes with PM to cause liver injury. Further analysis of metabolomic characterization of the liver injury phenotype revealed substantial modifications in the metabolic profiles of the TPH group compared to controls. Crucially, the metabolic signature of the TPH group was distinct from that induced by TNF-α or PM alone. To eliminate the individual effects of TNF-α or PM on the body, we subtracted the variables between the PH group vs N and the TNF-α group vs N from the common variables of the TPH group vs N, the PH group vs N and the TNF-α group vs N. By this method, we pinpointed 18 differential metabolites specifically associated with the synergistic liver injury under the combined influence of susceptibility factors and drugs. Among these, notable changes were observed in key metabolites such as reduced GSH, Inosine, Uric acid and 20-HETE metabolites in the TPH group showed significant changes compared with those in the N group, suggesting that they may be the material basis for the exacerbation of liver injury under immune stress conditions. In addition, the metabolite pathway enrichment analysis showed that the metabolomic characteristics of TNF-α-mediated PM-induced IDILI mainly involved glutathione metabolism, purine metabolism, and arachidonic acid metabolism.

[39] GSH, a tripeptide consisting of glutamate, cysteine and glycine, plays a vital role in oxidative metabolism and also serves as a constituent of the antioxidant defense mechanism.[40,41] GSH is a critical intracellular antioxidant in detoxification processes, including toxins, pollutants and drugs.[42,43] The observed alterations related to GSH metabolism in the TPH group align with this concept, suggesting impaired antioxidant defense or detoxification capacity contributes to the injury. Inosine, an intermediate in purine metabolism, has complex roles, with some studies suggesting protective effects against liver injury via gut microbiota modulation.[44] Depletion of GSH can impair mitochondrial function and increase cellular susceptibility to toxicants, potentially worsening drug-induced hepatotoxicity. This is consistent with the results of this study. Inosine is an important mediator of the purine biosynthesis pathway and a secondary metabolite of purine degradation.[45] Previous studies have reported that Inosine pretreatment can alter the intestinal flora structure and ameliorate LPS-induced acute liver injury and inflammation.[46] Uric acid, the end product of purine degradation, was elevated in the TPH group.[47–49] Substantial evidence that high Uric acid levels are closely associated with various liver diseases, including fatty liver disease, alcoholic liver disease, and acute liver injury.[50,51] 20-HETE, an ω-hydroxylated metabolite of arachidonic acid, is involved in regulating vascular tone and inflammation. The elevated levels are associated with various cardiometabolic diseases such as hypertension, obesity and metabolic syndrome, myocardial infarction, stroke and chronic kidney disease.[52] Arachidonic acid metabolism itself is implicated in diverse physiological and pathological processes, including inflammation and potentially liver homeostasis.[53] Collectively, these metabolic shifts suggest that arachidonic acid attenuates cholestatic liver disease by upregulating Oatp1, promoting the absorption of bile acid by hepatocytes and participating in entero-hepatic circulation. Therefore, we suggest that under conditions of TNF-α-mediated immune stress, PM can affect the changes in the levels of multiple metabolites and alters metabolic pathways such as glutathione metabolism, purine metabolism, and arachidonic acid metabolism to cause IDILI.

Microbiota and metabolic correlation analysis revealed relationships between key gut flora and potential metabolites associated with liver injury at the generic level. The positive correlation between *Akkermansia* and GSH aligns with reports where *Akkermansia* administration mitigated oxidative stress (eg, in acetaminophen-induced injury) by potentially supporting GSH balance between GSH, Uric acid, 3′-Dephosphocoenzyme A, and gamma-Glutamylcysteine.[35] Previous studies have reported that *Akkermansia* administration attenuated APAP-induced oxidative stress and inflammation significantly, restored the reduced glutathione/glutathione oxide (GSH/GSSG) balance, and effectively alleviated APAP-induced hepatotoxicity.[54] *Firmicutes* affect glutathione (GSH) de novo synthesis by regulating the subunit of glutamate-cysteine ligase catalytic (Gclc), which is a key enzyme of glutathione (GSH). It inhibits mitochondrial biogenesis and ROS accumulation via the cAMP reaction element binding (CREB) pathway. Thus, PM may contribute

to IDILI through TNF-α-mediated disturbances in glutathione metabolism, purine metabolism, and gut microbial abundance. Meanwhile, we also believe that this method may be applicable to other traditional Chinese medicines with the risk of IDILI, but the specific mechanism still needs to be verified through a large number of experiments and clinical studies.

Conclusions

In summary, the study highlights TNF-α as a critical susceptibility-related factor for PM-DILI in mice. We further elucidated the potential interactions, demonstrating that co-exposure to TNF-α and PM leads to significant alterations in the gut microbiota, characterized notably by disrupting the homeostasis of the intestinal flora (significantly reducing *Akkermansia* and increasing *Lachnospiraceae_NK4A136_group*, Bacteroides, Alloprevotella, and Blautia). This dysbiosis drives glutathione depletion, purine metabolism dysfunction, and 20-HETE accumulation, creating a vicious cycle of oxidative stress and inflammation that exacerbates liver injury. In the future, it is necessary to expand the sample size and further explore the changes in specific intestinal flora metabolites after the combination of TNF-α and PM through mechanism verification and clinical intervention, to achieve the transformation from correlation to causality. These findings contribute to risk management research in PM, as well as providing a direction and idea for the mechanism research of IDILI.

Acknowledgments

This study was supported by the National Natural Science Foundation of China (Grant No. 82204752), the Southwest Minzu University Research Startup Funds (Grant No. RQD2021057), and the Fundamental Research Funds for the Central Universities, Southwest Minzu University (Grant No. ZYN2023082).

Disclosure

The authors report no conflicts of interest in this work.

References

1. Zeo-Sánchez DE, Segovia-Zafra A, Matilla-Cabello G, et al. Modeling drug-induced liver injury: current status and future prospects. *Expert Opin Drug Metab Toxicol*. 2022;18(9):555–573. doi:10.1080/17425255.2022.2122810
2. Román-Sagüillo S, Quiñones Castro R, Juárez-Fernández M, et al. Idiosyncratic drug-induced liver injury and amoxicillin-clavulanate: spotlight on gut microbiota, fecal metabolome and bile acid profile in patients. *Int J Mol Sci*. 2024;25(13):6863. doi:10.3390/ijms25136863
3. Segovia-Zafra A, Villanueva-Paz M, Serras AS, et al. Control compounds for preclinical drug-induced liver injury assessment: consensus-driven systematic review by the ProEuroDILI network. *J Hepatol*. 2024;81(4):630–640. doi:10.1016/j.jhep.2024.04.026
4. Fontana RJ, Bjornsson ES, Reddy R, Andrade RJ. The evolving profile of idiosyncratic drug-induced liver injury. *Clin Gastroenterol Hepatol*. 2023;21(8):2088–2099. doi:10.1016/j.cgh.2022.12.040
5. Devarbhavi H, Asrani SK, Arab JP, Nartey YA, Pose E, Kamath PS. Global burden of liver disease: 2023 update. *J Hepatol*. 2023;79(2):516–537. doi:10.1016/j.jhep.2023.03.017
6. Chen M, Suzuki A, Borlak J, Andrade RJ, Lucena MI. Drug-induced liver injury: interactions between drug properties and host factors. *J Hepatol*. 2015;63(2):503–514. doi:10.1016/j.jhep.2015.04.016
7. Lu J, Jones AD, Harkema JR, Roth RA, Ganey PE. Amiodarone exposure during modest inflammation induces idiosyncrasy-like liver injury in rats: role of tumor necrosis factor-alpha. *Toxicol Sci*. 2012;125(1):126–133. doi:10.1093/toxsci/kfr266
8. Wang Y, Xu G, Wang Z, et al. Psoralidin, a major component of Psoraleae Fructus, induces inflammasome activation and idiosyncratic liver injury. *Int Immunopharmacol*. 2021;92:107352. doi:10.1016/j.intimp.2020.107352
9. Wang Z, Xu G, Wang H, et al. Icariside II, a main compound in Epimedii Folium, induces idiosyncratic hepatotoxicity by enhancing NLRP3 inflammasome activation. *Acta Pharm Sin B*. 2020;10(9):1619–1633. doi:10.1016/j.apsb.2020.03.006
10. Xue X, Quan Y, Gong L, Gong X, Li Y. A review of the processed Polygonum multiflorum (Thunb.) for hepatoprotection: clinical use, pharmacology and toxicology. *J Ethnopharmacol*. 2020;261:113121. doi:10.1016/j.jep.2020.113121
11. Lei X, Chen J, Ren J, et al. Liver Damage Associated with Polygonum multiflorum Thunb.: a Systematic Review of Case Reports and Case Series. *Evid Based Complement Alternat Med*. 2015;2015:459749. doi:10.1155/2015/459749
12. Wang Y, Wang L, Saxena R, et al. Clinicopathological features of He Shou Wu-induced liver injury: this ancient anti-aging therapy is not liver-friendly. *Liver Int*. 2019;39(2):389–400. doi:10.1111/liv.13939
13. Chalasani NP, Maddur H, Russo MW, Wong RJ, Reddy KR. ACG clinical guideline: diagnosis and management of idiosyncratic drug-induced liver injury. *Am J Gastroenterol*. 2021;116(5):878–898. doi:10.14309/ajg.0000000000001259
14. Gong L, Shen X, Huang N, et al. Research progress on hepatotoxicity mechanism of polygonum multiflorum and its main components. *Toxicon*. 2024;248:108040. doi:10.1016/j.toxicon.2024.108040
15. Li C, Rao T, Chen X, et al. HLA-B*35:01 allele is a potential biomarker for predicting Polygonum Multiflorum-induced liver injury in humans. *Hepatology*. 2019;70(1):346–357. doi:10.1002/hep.30660

16. Rao T, Liu YT, Zeng XC, Li CP, Ou-Yang DS. The hepatotoxicity of Polygonum multiflorum: the emerging role of the immune-mediated liver injury. *Acta Pharmacol Sin*. 2021;42(1):27–35. doi:10.1038/s41401-020-0360-3
17. Wu X, Zhang Y, Qiu J, et al. Lipidomics analysis indicates disturbed hepatocellular lipid metabolism in reynoutria multiflora-induced idiosyncratic liver injury. *Front Pharmacol*. 2020;11:569144. doi:10.3389/fphar.2020.569144
18. Tu C, Niu M, Wei AW, et al. Susceptibility-related cytokine panel for prediction of polygonum multiflorum-induced hepatotoxicity in humans. *J Inflamm Res*. 2021;14:645–655. doi:10.2147/JIR.S299892
19. Zhang L, Niu M, Wei AW, et al. Risk profiling using metabolomic characteristics for susceptible individuals of drug-induced liver injury caused by Polygonum multiflorum. *Arch Toxicol*. 2020;94(1):245–256. doi:10.1007/s00204-019-02595-3
20. Zhang L, Niu M, Wei AW, et al. Clinical correlation between serum cytokines and the susceptibility to Polygonum multiflorum-induced liver injury and an experimental study. *Food Funct*. 2022;13(2):825–833. doi:10.1039/D1FO03489H
21. Albillos A, de Gottardi A, Rescigno M. The gut-liver axis in liver disease: pathophysiological basis for therapy. *J Hepatol*. 2020;72(3):558–577. doi:10.1016/j.jhep.2019.10.003
22. Tripathi A, Debelius J, Brenner DA, et al. The gut-liver axis and the intersection with the microbiome. *Nat Rev Gastroenterol Hepatol*. 2018;15(7):397–411. doi:10.1038/s41575-018-0011-z
23. Wang R, Tang R, Li B, Ma X, Schnabl B, Tilg H. Gut microbiome, liver immunology, and liver diseases. *Cell Mol Immunol*. 2021;18(1):4–17. doi:10.1038/s41423-020-00592-6
24. Cani PD, Moens de Hase E, Van Hul M. Gut microbiota and host metabolism: from proof of concept to therapeutic intervention. *Microorganisms*. 2021;9(6):1302. doi:10.3390/microorganisms9061302
25. Wahlström A, Sayin SI, Marschall HU, Bäckhed F. Intestinal crosstalk between bile acids and microbiota and its impact on host metabolism. *Cell Metab*. 2016;24(1):41–50. doi:10.1016/j.cmet.2016.05.005
26. Zmora N, Zilberman-Schapira G, Suez J, et al. Personalized gut mucosal colonization resistance to empiric probiotics is associated with unique host and microbiome features. *Cell*. 2018;174(6):1388–1405.e1321. doi:10.1016/j.cell.2018.08.041
27. Koh A, De Vadder F, Kovatcheva-Datchary P, Bäckhed F. From dietary fiber to host physiology: short-chain fatty acids as key bacterial metabolites. *Cell*. 2016;165(6):1332–1345. doi:10.1016/j.cell.2016.05.041
28. Tukov FF, Luyendyk JP, Ganey PE, Roth RA. The role of tumor necrosis factor alpha in lipopolysaccharide/ranitidine-induced inflammatory liver injury. *Toxicol Sci*. 2007;100(1):267–280. doi:10.1093/toxsci/kfm209
29. Shaw PJ, Hopfensperger MJ, Ganey PE, Roth RA. Lipopolysaccharide and trovafloxacin coexposure in mice causes idiosyncrasy-like liver injury dependent on tumor necrosis factor-alpha. *Toxicol Sci*. 2007;100(1):259–266. doi:10.1093/toxsci/kfm218
30. Zou W, Beggs KM, Sparkenbaugh EM, et al. Sulindac metabolism and synergy with tumor necrosis factor-alpha in a drug-inflammation interaction model of idiosyncratic liver injury. *J Pharmacol Exp Ther*. 2009;331(1):114–121. doi:10.1124/jpet.109.156331
31. Chopyk DM, Grakoui A. Contribution of the intestinal microbiome and gut barrier to hepatic disorders. *Gastroenterology*. 2020;159(3):849–863. doi:10.1053/j.gastro.2020.04.077
32. Cani PD, Van Hul M, Lefort C, Depommier C, Rastelli M, Everard A. Microbial regulation of organismal energy homeostasis. *Nat Metab*. 2019;1(1):34–46. doi:10.1038/s42255-018-0017-4
33. Levy M, Kolodziejczyk AA, Thaiss CA, Elinav E. Dysbiosis and the immune system. *Nat Rev Immunol*. 2017;17(4):219–232. doi:10.1038/nri.2017.7
34. Parada Venegas D, De la Fuente MK, Landskron G, et al. Short Chain Fatty Acids (SCFAs)-mediated gut epithelial and immune regulation and its relevance for inflammatory bowel diseases. *Front Immunol*. 2019;10:277.
35. Xia J, Lv L, Liu B, et al. Akkermansia muciniphila ameliorates acetaminophen-induced liver injury by regulating gut microbial composition and metabolism. *Microbiol Spectr*. 2022;10(1):e0159621. doi:10.1128/spectrum.01596-21
36. Zhuge A, Li S, Lou P, et al. Longitudinal 16S rRNA sequencing reveals relationships among alterations of gut microbiota and nonalcoholic fatty liver disease progression in mice. *Microbiol Spectr*. 2022;10(3):e0004722. doi:10.1128/spectrum.00047-22
37. Huang X, Jin Y, Wang T, et al. WED-541 gut akkermansia improves liver injury in D-penicillamine treated copper exposure model. *J Hepatol*. 2024;80:S280. doi:10.1016/S0168-8278(24)01018-3
38. Perino A, Demagny H, Schoonjans K. A microbial-derived succinylated bile acid to safeguard liver health. *Cell*. 2024;187(11):2687–2689. doi:10.1016/j.cell.2024.04.020
39. Niu B, Liao K, Zhou Y, et al. Application of glutathione depletion in cancer therapy: enhanced ROS-based therapy, ferroptosis, and chemotherapy. *Biomaterials*. 2021;277:121110. doi:10.1016/j.biomaterials.2021.121110
40. Jiang X, Du B, Zheng J. Glutathione-mediated biotransformation in the liver modulates nanoparticle transport. *Nat Nanotechnol*. 2019;14(9):874–882. doi:10.1038/s41565-019-0499-6
41. Pathania S, Bhatia R, Baldi A, Singh R, Rawal RK. Drug metabolizing enzymes and their inhibitors' role in cancer resistance. *Biomed Pharmacother*. 2018;105:53–65. doi:10.1016/j.biopha.2018.05.117
42. Averill-Bates DA. The antioxidant glutathione. *Vitam Horm*. 2023;121:109–141.
43. Ferreira J. Glutathione is essential for liver lipid metabolism. *Lab Anim*. 2024;53(9):219.
44. Vairetti M, Di Pasqua LG, Cagna M, Richelmi P, Ferrigno A, Berardo C. Changes in glutathione content in liver diseases: an update. *Antioxidants*. 2021;10(3). doi:10.3390/antiox10030364
45. Guo W, Xiang Q, Mao B, et al. Protective effects of microbiome-derived inosine on lipopolysaccharide-induced acute liver damage and inflammation in mice via mediating the TLR4/NF-κB pathway. *J Agric Food Chem*. 2021;69(27):7619–7628. doi:10.1021/acs.jafc.1c01781
46. Xie D, Zhao H, Lu J, et al. High uric acid induces liver fat accumulation via ROS/JNK/AP-1 signaling. *Am J Physiol Endocrinol Metab*. 2021;320(6):E1032–e1043. doi:10.1152/ajpendo.00518.2020
47. Tang C, Cen L, Zeng H, et al. Inhibiting hepatocyte uric acid synthesis and reabsorption ameliorates acetaminophen-induced acute liver injury in mice. *Cell Mol Gastroenterol Hepatol*. 2024;17(2):251–265. doi:10.1016/j.jcmgh.2023.10.005
48. Wang M, Chen WY, Zhang J, et al. Elevated fructose and uric acid through aldose reductase contribute to experimental and human alcoholic liver disease. *Hepatology*. 2020;72(5):1617–1637. doi:10.1002/hep.31197
49. Zeng H, Tang C, Lin B, et al. The regulation effect of GLUT9/SLC2A9 on intrahepatic uric acid level and metabolic associated fatty liver disease. *Hepatol Int*. 2022;16(5):1064–1074. doi:10.1007/s12072-022-10371-2

50. Rocic P, Schwartzman ML. 20-HETE in the regulation of vascular and cardiac function. *Pharmacol Ther*. 2018;192:74–87. doi:10.1016/j.pharmthera.2018.07.004
51. Roman RJ. 20-HETE and Hypertension. *Hypertension*. 2024;81(10):2012–2015. doi:10.1161/HYPERTENSIONAHA.124.21718
52. Hu Y, Li W, Cheng X, et al. Emerging roles and therapeutic applications of arachidonic acid pathways in cardiometabolic diseases. *Circ Res*. 2024;135(1):222–260. doi:10.1161/CIRCRESAHA.124.324383
53. Ma Y, Zou C, Yang Y, et al. Arachidonic acid enhances hepatocyte bile acid uptake and alleviates cholestatic liver disease by upregulating OATP1 expression. *Food Funct*. 2024;15(19):9916–9927. doi:10.1039/D4FO02158D
54. Yuan Y, Yang J, Zhuge A, Li L, Ni S. Gut microbiota modulates osteoclast glutathione synthesis and mitochondrial biogenesis in mice subjected to ovariectomy. *Cell Prolif*. 2022;55(3):e13194. doi:10.1111/cpr.13194